RSC Advances

PAPER

View Article Online
View Journal | View Issue

Cite this: *RSC Adv.*, 2025, **15**, 44061

Green synthesis of CuO nanoparticles using *Aegle marmelos* fruit pulp extract: a sustainable approach for biomedical and supercapacitor applications

Anil B. Patil,[a] Vaibhav B. Sankpal,[a] Omkar S. Nille,[b] Rajesh C. Waghmare,[a] Vishakha S. Parkhe,[c] Arpita Pandey-Tiwari,[c] Govind B. Kolekar,[b] Asha D. Patil*[d] and Gopinath S. Khansole *[a]

This study presents a green and eco-friendly approach to synthesize copper oxide (CuO) nanoparticles (NPs) using *Aegle marmelos* fruit pulp extract as a natural reducing and stabilizing agent. In this study, *Aegle marmelos*, known for its rich phytochemical profile, including flavonoids, phenolics, and tannins, was employed to reduce copper sulphate to CuO NPs. The synthesized NPs were characterized using Fourier transform infrared (FTIR) spectroscopy, X-ray diffraction (XRD), Raman spectroscopy, scanning electron microscopy (SEM), transmission electron microscopy (TEM), X-ray photoelectron spectroscopy (XPS), and electrochemical measurements. The monoclinic phase, nano-crystalline structure, and presence of bioactive compounds from the extract acting as capping and stabilizing agents were confirmed by XRD, FTIR, and Raman spectroscopy. The synthesized CuO NPs were evaluated for antibacterial, antioxidant, and hemolytic activity. Furthermore, the electrochemical performance of the CuO-based electrode was investigated to explore its potential applications in supercapacitors.

Received 16th September 2025
Accepted 14th October 2025

DOI: 10.1039/d5ra07029e

rsc.li/rsc-advances

1. Introduction

Nanotechnology is a rapidly growing discipline that has a significant impact on many aspects of human existence, including food, pharmaceuticals, health electronics, chemical industry, energy, cosmetics, space, and environmental sciences.[1] One of the most captivating aspects of cutting-edge studies is the synthesis of nanomaterials and the exploration of their uses and characteristics.[2] A nanoparticle is a term used to describe a particle of matter with a diameter in the range of 1 to 100 nm. There are only two orientations for particles up to 500 nm or for fibers and tubes smaller than 100 nm.[3] Most of the time, NPs are distinguished from micro particles (1–1000 μm) due to their smaller size. Fine particles (between 100 and 2500 nm) and coarse particles (between 2500 and 10 000 nm) have highly diverse physical and chemical properties, such as colloidal properties, ultrafast optical effects, and electric properties.[4] Silver, zinc, and gold metal NPs have been utilized as therapeutic agents in medical facilities for several years.[5] Transitional metal oxides, including CuO, TiO_2, Fe_3O_4, ZnO, and NiO NPs, have demonstrated successful use as cutting-edge nanomaterials in the domains of energy, biomedicine, and environment. The performance and applicability of these NPs are significantly enhanced by their excellent adsorption capabilities.[6] A few recent studies reported that among metal oxides, copper oxide (CuO) is a p-type semiconductor with a bandgap of 1.2 eV whose improved biological and photocatalytic activities are superior to those obtained from metal NPs.[7,8]

There are various methods for synthesizing metal oxide-based NPs, including sol–gel, hydrothermal, sonication, and coprecipitation. These methods are very expensive, require the use of harmful chemicals, are time-consuming, and produce toxic byproducts. Consequently, developing environmentally acceptable procedures has become crucial for the synthesis of nanomaterials. CuO is utilized in various applications, including in heterogeneous catalysts,[9] solar energy conversion,[10] field emitters,[11] electrode materials in lithium-ion batteries,[12] and gas sensors.[13] Superconducting resources, glass, thermoelectric materials, and antimicrobial activities.[14,15] To the best of our knowledge, green synthesis is the most appropriate and straightforward fabrication method when environmental concerns are considered because it is nontoxic, environmentally friendly, and advantageous due to its straightforward reaction setup and reasonably priced reaction parameters.[16]

[a]*Department of Chemistry, Deshbhakt Anandrao Balwantrao Naik Arts and Science College, Chikhali, Sangli-415408, Affiliated to Shivaji University, Kolhapur, MH, India. E-mail: gopinathskhansole@gmail.com*

[b]*Fluorescence Spectroscopy Research Laboratory, Department of Chemistry, Shivaji University, Kolhapur-416004, MH, India*

[c]*Department of Medical Biotechnology and Stem Cells and Regenerative Medicine, Centre for Interdisciplinary Research, D. Y. Patil Education Society, Kolhapur-416006, MH, India. E-mail: arpitaptiwari@gmail.com*

[d]*Department of Physics, Deshbhakt Anandrao Balwantrao Naik Arts and Science College, Chikhali, Sangli-415408, Affiliated to Shivaji University, Kolhapur, MH, India. E-mail: ashapatil2577@gmail.com*

CuO NPs made from *Psoralea corylifolia* seed extract exhibited excellent anticancer activity,[17] while colour degradation was evaluated using *Avicennia marina* flower extract,[18] and antibacterial and photocatalytic activities were studied by employing the plant extract of *Kappaphycus alvarezii*.[19] Furthermore, the antibacterial activity of CuO NPs prepared from the leaf extract of *Averrhoa carambola* was evaluated against the bacterial strains *Salmonella typhi*, *Pseudomonas aeruginosa*, *Escherichia coli*, *Staphylococcus aureus*, and *Bacillus megaterium*. High zones of inhibition were found at 26 and 24 nm against *Salmonella typhi* and *Escherichia coli*, respectively.[20]

To synthesize CuO NPs, plant materials, such as *Euphorbia nivulia* stem latex and magnolia leaf extract, were used, and these NPs exhibited exceptional antibacterial activity against *Escherichia coli cells*. Furthermore, NPs were employed as harmless aqueous formulations for cancer treatment.[21,22] CuO NPs were produced environmentally by employing an aqueous extract of the *Cedrus deodara* tree, which acted as a non-toxic and low-cost reducing agent. The study focuses on the potential of these NPs for biomedical and pharmaceutical applications due to their efficiency and low toxicity.[19] The green synthesis method is used to synthesize CuO NPs from the leaf extract of the *Maura sylvestris* tree. Research has shown the potential of CuO NPs to enhance the thermal characteristics of nitrocellulose.[21] Copper oxide NPs prepared from *Aegle marmelos* leaf extract exhibit significant cytotoxicity, particularly at an IC_{50} concentration of 25 mg mL^{-1} and NPs can promote oxidative stress and cell death in colorectal cancer cells.[22] The green synthesis of CuO NPs using 10% fruit pulp extract from *Aegle marmelos* is the aim of this study. The formed CuO NPs were assessed for their antibacterial, antioxidant, and haemolytic properties. The CuO-based electrode's electrochemical performance was further investigated to determine its potential use in supercapacitors.

2. Experimental

2.1. Chemicals

AR grade cupric sulphate pentahydrate ($CuSO_4 \cdot 5H_2O$) was used in the present study (SRL, PVT, LTD). Double-distilled water was used throughout the investigation process. 1,1-Diphenyl-2-picrylhydrazyl (DPPH) and methanol were obtained from HiMedia Laboratories Pvt. Ltd. All other chemicals used in the experiment were of analytical grade.

2.2. Collection and preparation of fruit pulp extracts

Fresh Fruits of *Aegle marmelos* were collected from the Sangli district, Maharashtra. Initially, fully ripe *Aegle marmelos* fruits, which have a yellowish-brown outer shell and a fragrant aroma, were selected. These fruits were opened using a hammer or a sharp knife. Then, pulp was extracted from ripe *Aegle marmelos* fruit. Furthermore, 10 g of pulp was added to 100 mL of double-distilled water and heated at 60–70 °C for 1 hour with stirring. Then, it was allowed to cool, and the extract was filtered using Whatman filter paper. The fresh pulp was stored in a clean airtight container in the refrigerator (3–5 days).

2.3. Green synthesis of CuO NPs

To synthesize CuO nanoparticles from the *Aegle marmelos* fruit pulp extract, 20 mL of $CuSO_4$ solution was added into the *Aegle marmelos* extract, and the suspension was stirred on a magnetic stirrer for 1–2 hours at room temperature. Then, the colour of the solution was changed from blue to dark green/black, indicating the formation of CuO NPs. Then, 10–11 pH of the solution was adjusted by dropwise addition of concentrated ammonia. After stirring, the reaction mixture was left undisturbed at room temperature for 24 hours. Furthermore, the solution was centrifuged at 8000 rpm for 10 minutes to collect the precipitate, after which it was washed with distilled water and ethanol to remove impurities and unreacted components. Besides, the precipitate was dried in a hot air oven at 80–100 °C for 4–6 hours to remove residual moisture. The dry powder was calcinated for 4–5 hours at 300 °C.

2.4. Antibacterial activity

The antibacterial efficacy of CuO NPs was investigated using the agar well diffusion assay. This method was used against clinically isolated bacterial cultures, including Gram-positive (*Staphylococcus aureus*) and Gram-negative (*Escherichia coli* and *Klebsiella pneumoniae*). In brief, 50 μL of the mother cultures of each inoculum were uniformly spread on individual sterile nutrient agar plates. The wells were punctured on agar plates using a sterile stainless-steel well puncher (5 mm diameter). The 80 μg and 100 μg of the CuO NPs were added to the well under aseptic conditions. Sterile distilled water was used as a negative control, and a standard antibiotic (Penstrep) was used as a positive control. The plates were incubated at 37 °C for 24 h. The zone of inhibition (in millimeters (mm)) around the well loaded with the specified concentrations of CuO NPs was measured to determine the antibacterial efficacy for each clinical strain.[23]

2.5. Antioxidant activity

2.5.1. DPPH free radical scavenging assay. The anti-oxidant activity of CuO NPs was determined using the DPPH free radical scavenging assay. First, 0.78 mg of DPPH was added to 10 mL of methanol to create a stock solution. DPPH solution (100 μL) was applied to each CuO NP well at concentrations of 20, 40, 60, 80, and 100 μg mL^{-1}. The reaction mixture was agitated for 5 minutes and then incubated in a dark place at room temperature for 30 minutes. The absorbance of the resultant solution was measured at 517 nm. Ascorbic acid was employed as a positive control.[24] All experiments were carried out in triplicate, and the percentage of anti-oxidation was calculated using the following formula:

$$\text{DPPH free radical scavenging}(\%) = \frac{\text{Control absorbance} - \text{Sample absorbance}}{\text{Control absorbance}} \times 100. \quad (1)$$

The control absorbance reflects the maximum absorbance at zero minutes, while the sample absorbance reflects the maximum absorbance at the specified period.

2.6. Haemolytic activity

Human blood hemolysis experiments were conducted to assess the reaction of human red blood cells in contact with CuO NPs. A 5 mL blood sample was obtained from a healthy volunteer and preserved in EDTA-coated K2 tubes with anticoagulant to avoid clotting of the sample. Following that, the blood sample was centrifuged at 3000 rpm for 15 minutes, and the levels of hematocytes were determined to separate the plasma in a container. The cells were then rinsed three times with repeated centrifugation. The volume of the obtained red blood cells was analyzed, and a 10% v/v working solution was prepared by diluting it with a 0.95% normal saline solution. After that, different concentrations of CuO NPs (20, 40, 60, 80, and 100 μg mL^{-1}), negative control (NC), and positive control (PC) were prepared. Then, each centrifuge tube was filled with 0.5 mL of diluted blood and 0.5 mL of varied concentrations of CuO NPs and incubated at 37 °C for 1–4 hours. To create positive controls, 0.5 mL of diluted blood was added to the distilled water. In contrast, 0.5 mL of diluted blood in 0.5 mL of normal saline served as a negative control. The sample was vortexed and centrifuged at 3000 rpm for 10 minutes. The supernatant was collected, and absorbance was measured at 540 nm with a microplate reader (Skanlt RE 6.1). All experiments were carried out in triplicate, and the percentage inhibition was calculated using the following formula:[25,26]

$$\%\ \text{of inhibition of hemolysis} = \frac{\text{Absorbance of sample} - \text{Absorbance of NC}}{\text{Absorbance of PC} - \text{Absorbance of NC}} \times 100. \quad (2)$$

2.7. Characterization of synthesized CuO nanoparticles

The XRD patterns for the investigated samples were obtained using an X-ray diffractometer (Bruker-AXS D8 Advance) in a 2θ range of 20–80° with Cu Kα radiation at room temperature (λ = 1.5405 Å). FTIR spectra of plant leaf extract and synthesized copper oxide nanoparticles were obtained in the range of 4000–400 cm^{-1} using the KBr pellet method. To analyze the surface morphology, SEM images were obtained using a field-emission scanning electron microscope. Fourier transform infrared (FTIR) spectroscopy was employed to investigate the functional groups present in the sample. The vibrational modes of the prepared samples were studied using Raman spectroscopy (INCIA0120-20, Renishaw). The morphology, shape, and size of the CuO NPs were evaluated using TEM analysis (JEOL, voltage of 300 kV). The elemental analysis of CuO NPs was performed with X-ray Photoelectron Spectroscopy (XPS) over a binding energy range of 0–800 eV using Mg Kα (1253.6 eV) as an X-ray source (JEOL, JPS 9030).

2.8. Electrochemical measurements

The present report utilizes a three-electrode configuration system to analyse the performance and stability of materials. The electrolyte used for conducting cyclic voltammetry (CV) and galvanic charge–discharge measurements (GCD) was a 1 M solution of sodium sulphate (Na_2SO_4) in water. In the electrochemical experiments, the reference electrode is a standard Ag–AgCl electrode, and the counter electrode utilized is a platinum wire. All measurements, including CV and GCD, were conducted at room temperature using Metrohm Auto Lab Potentiostat/Galvanostat instruments.

3. Results and discussion

3.1. XRD analysis

The crystal structure of the prepared samples was confirmed by their XRD patterns. The XRD patterns of CuO NPs investigated using 10% of *Aegle marmelos* fruit pulp extract calcined at 500 °C are depicted in Fig. 1. The X-ray diffraction pattern was recorded in the range of 20–80°. In the present work, the peak positions observed at 2θ = 32.53°, 35.74°, 38.95°, 48.94, 53.59°, 58.59°, 66.52°, and 68.04° matched the (110), (−111), (111), (−202), (112), (202), (022), and (220) planes, respectively. The crystalline nature, as well as the monoclinic structure, of the synthesized samples was indicated by the presence of sharp peaks in the diffraction patterns. No other phases were observed, indicating the phase purity of the investigated CuO NPs. The crystallite size of the prepared sample was calculated using Debye–Scherer's equation:[27]

$$D = \frac{0.9\lambda}{\beta \cos\theta}, \quad (3)$$

where β is the full width at half-maximum (FWHM), λ is the wavelength of X-rays, and θ is the Bragg's angle. The computed crystalline size of green-synthesized CuO NPs using *Aegle marmelos* fruit pulp extract was 13 nm.

3.2. Scanning electron microscopy analysis

Scanning Electron Microscopy (SEM) was employed to study the surface morphology of the CuO NPs synthesized from *Aegle marmelos* fruit pulp extract. The SEM analysis provides insight into the surface texture, shape, and aggregation behavior of the NPs. Fig. 2 illustrates the SEM images of the CuO NPs. From the SEM image, it is observed that spherical-shaped particles are

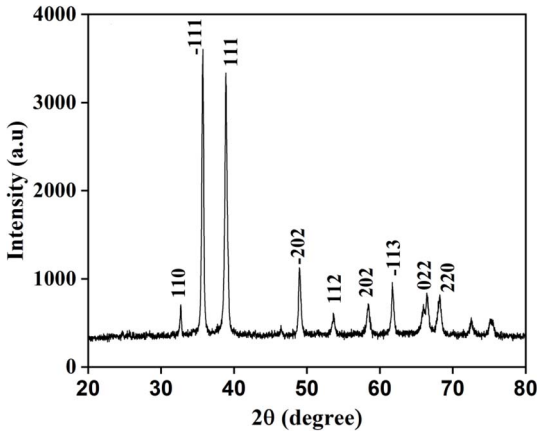

Fig. 1 XRD pattern of the synthesized CuO NPs.

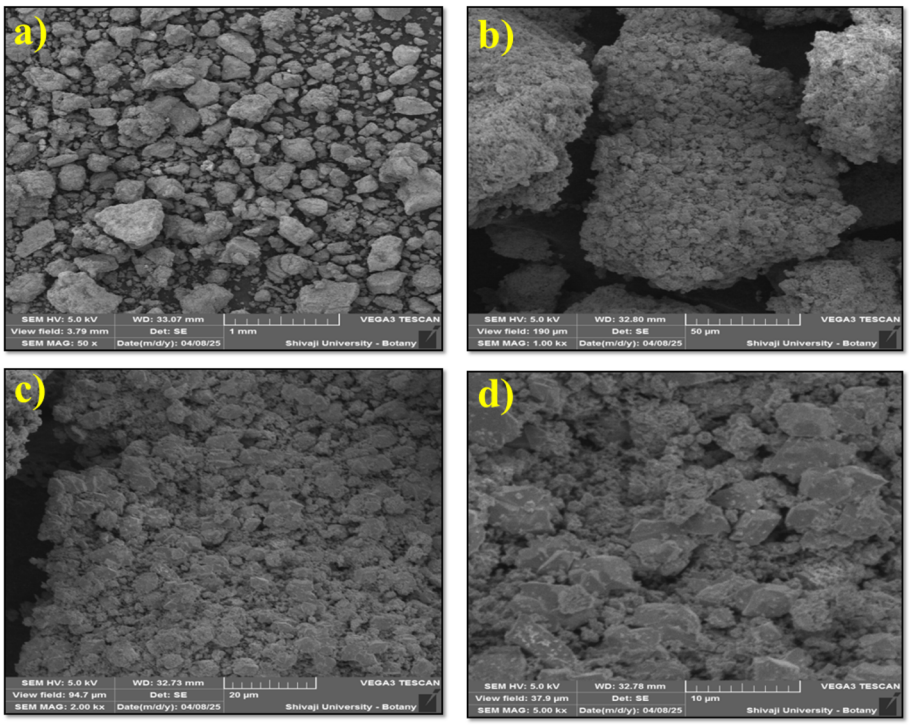

Fig. 2 (a–d) SEM images of the synthesized CuO NPs.

formed and agglomerated due to the oxidation of metal NPs, confirming the nanostructure behaviour.

3.3. Transmission electron microscopy analysis

The morphology, shape, and size of the synthesized CuO NPs were evaluated using TEM analysis. Fig. 3a shows the spherical morphology of the CuO NPs, with a uniform distribution. Further, Fig. 3b depicts the HR-TEM image with an interplanar spacing (d) of 0.12 nm. The selected area electron microscopic data show faded circular rings, suggesting the polycrystalline nature of CuO NPs, which matches well with the XRD analysis. The particle size of the CuO NPs ranged from 10 to 70 nm, with an average size of 35.86 nm.[28] The particle size and shape play a vital role in biomedical and energy applications.

3.4. X-ray photoelectron spectroscopy analysis

The survey spectrum of CuO was recorded over the range of 0–1000 eV, showing prominent peaks at binding energies of 77.50, 284.53, 532.50, 934.50, and 954.50 eV corresponding to the presence of Cu 1s, C 1s, O 1s, Cu $2p_{3/2}$ and Cu $2p_{1/2}$ elements, respectively (Fig. 4). The high-resolution survey spectra of C 1s were deconvoluted into four distinct peaks at 284.14 (C–H), 285.60 (C–C), 286.95 (C═C), and 294.36 (C═O) eV. The O 1s peak displayed two deconvoluted peaks at 528.69 eV (CuO), 531.15 (Cu_2O), and 533.30 (C–O/C═O). Furthermore, the sulfur shows three high-resolution peaks of C–S, S $2p_{3/2}$, and S $2p_{1/2}$ at binding energies of 162.72, 164.80, and 168.20 eV, respectively. Additionally, the Cu element shows four peaks at 934.90 Cu $2p_{3/2}$ (CuO), 942.55 Cu $2p_{3/2}$ (CuO), 954.10 Cu $2p_{1/2}$ (Cu_2O), and 962.21 $Cu(OH)_2$, respectively.[29,30]

3.5. Fourier transform infrared analysis

Fourier transform infrared spectroscopy was used to identify the functional groups that exist in the synthesized sample. Fig. 5 represents the FTIR spectra of synthesized CuO NPs between 400 and 4000 cm^{-1}. In the present spectra, various absorption peaks are observed at 537.89, 1020.74, 1634.48, 2350, and 3443.25 cm^{-1}. The broad band at 3443.25 cm^{-1} is related to the stretching mode of the hydroxyl group, which is attributed to the presence of atmospheric water during the analysis. The strong vibrational peak at 1020.74 cm^{-1} was attributed to the C–O–C bond stretches found in the ethers, while the carboxyl group was revealed at 1634.48 cm^{-1}. The peak at 537.89 cm^{-1} corresponds to Cu–O bond vibrational frequencies, confirming the formation of CuO NPs.[31,32] Similar results were also reported by various researchers, where CuO NPs were produced using different extracts of plants.[33–35]

3.6. Raman analysis

Raman spectroscopy was employed to confirm the phase and vibrational modes of the CuO NPs. Fig. 6 depicts the room temperature Raman spectra of synthesized CuO NPs in the range of 100–1000 cm^{-1}. The Raman peaks observed at 284 cm^{-1} and 325 cm^{-1} correspond to the fundamental Raman active mode of monoclinic CuO, while the peaks at 617 cm^{-1} and 1093 cm^{-1} are ascribed to higher overtone modes.

3.7. Antibacterial activity

The antibacterial activity of CuO NPs was studied against clinical strains, including Gram-positive (*Staphylococcus aureus*)

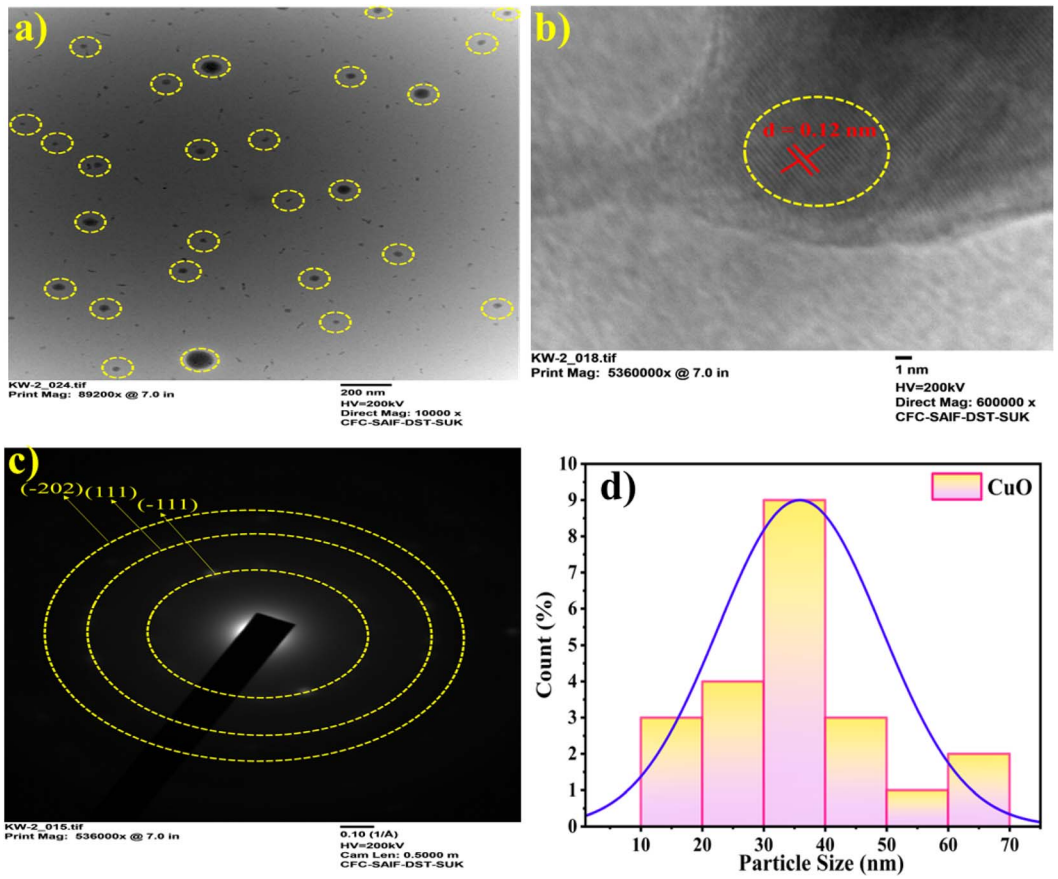

Fig. 3 (a and b) TEM images, (c) SAED pattern, and (d) particle size analysis of the CuO NPs.

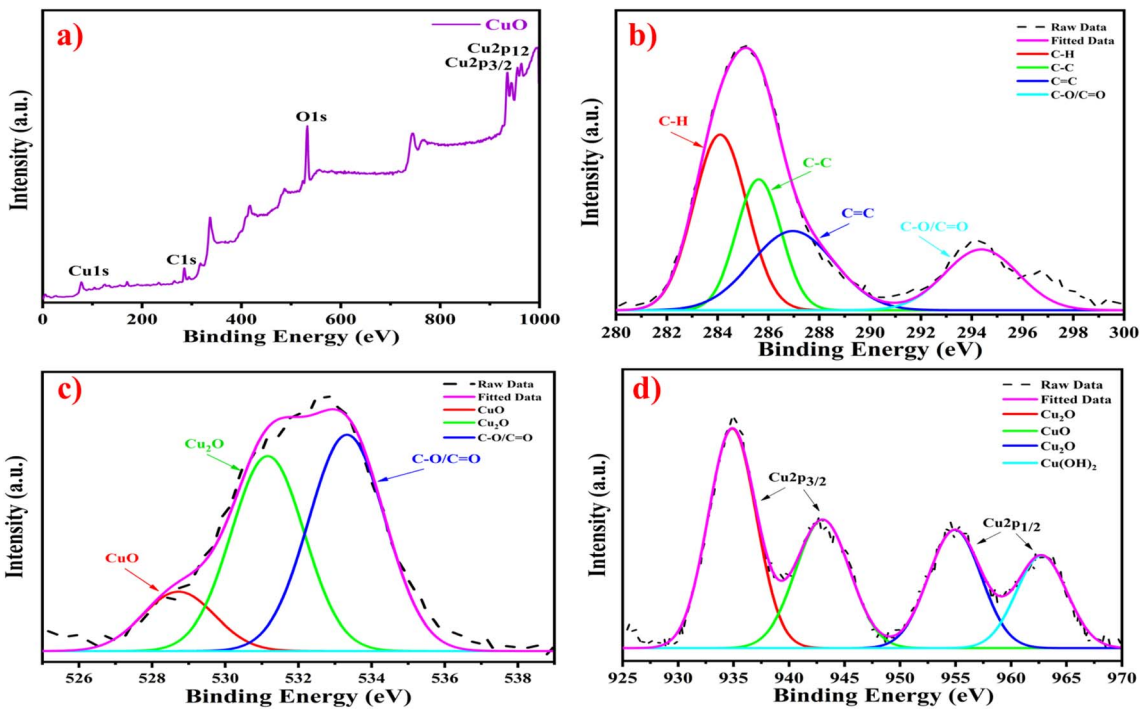

Fig. 4 (a) XPS survey spectra and high-resolution spectra of (b) C 1s, (c) O 1s and (d) Cu $2p_{3/2}$ and Cu $2p_{1/2}$.

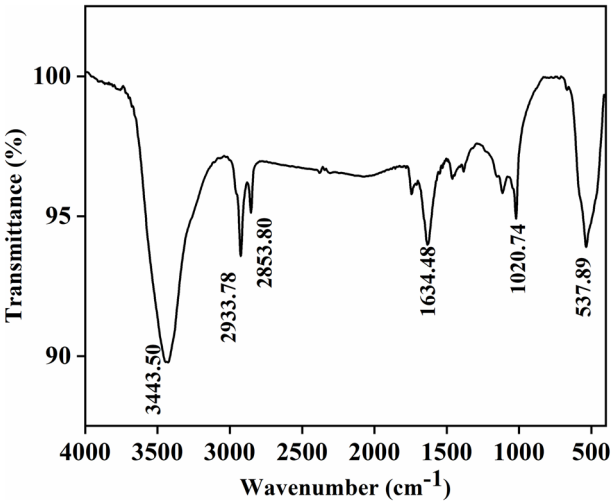

Fig. 5 FTIR spectrum of the synthesized CuO NPs.

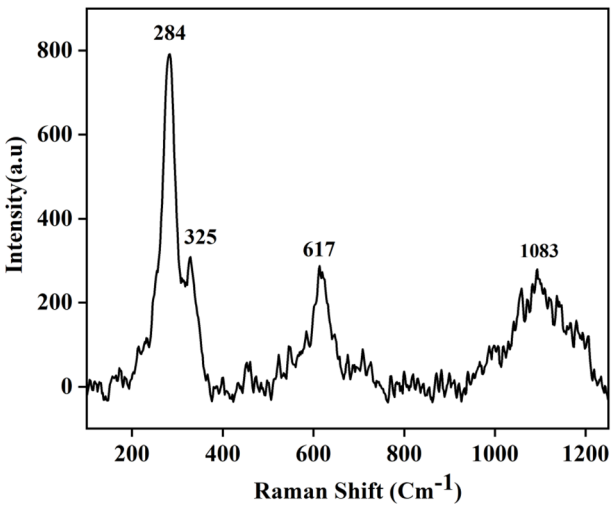

Fig. 6 Raman spectra of the synthesized CuO NPs.

and Gram-negative (*Escherichia coli* and *Klebsiella pneumoniae*) bacteria, using the agar well diffusion method, as shown in Fig. 7. Among all bacterial strains, the highest inhibitory activity of CuO NPs was observed against *Escherichia coli* (14 mm), followed by *Staphylococcus aureus* (13 mm) Table 1. Additionally, synthesized CuO NPs exhibited inhibitory activity against a multidrug-resistant bacterial strain, specifically *Klebsiella pneumoniae* (4 mm), at a concentration of 100 μg.

3.7.1. Possible mechanism of inhibitory activity of the CuO NPs. CuO NPs exhibit antimicrobial activity through direct interaction with bacterial cells, ROS formation, release of free copper cations, and interaction with biomolecules. In the present study, the possible mechanism of the inhibitory activity of CuO NPs is that transition metal cations, such as copper, have been shown to promote ROS production. During these reactions, the copper cation transfers electrons between Cu^{+} and Cu^{2+}, resulting in the generation of highly reactive superoxide anion radicals ($O_2^{\bullet -}$) and hydroxyl radicals ($^{\bullet}OH$). These species can oxidize nucleic acids, proteins, and lipids in bacterial cells.[36,37] CuO-NPs may exhibit antibacterial activity by releasing Cu^{+}/Cu^{2+} ions, which interact with bacterial cell surface molecules and membranes before being absorbed. The increased release of Cu^{2+} ions in the medium could be attributed to the oxide layer on the CuO-NPs and its interaction with Cl ions. Additionally, Cu^{2+} ions in the intracellular environment can damage double-stranded DNA by disrupting its helical shape. Binding can occur in phosphate groups and in large and small grooves in the DNA helix.[38]

3.8. Antioxidant activity

DPPH is a well-known free radical that has been linked to cell damage. Metal NPs can neutralize damaging free radicals, such as DPPH. DPPH's scavenging method involves forming the non-radical form of DPPH-H in the presence of hydrogen-donating antioxidants. These antioxidants play a critical role in eliminating free radicals. CuO NPs possess high antioxidant properties that reduce oxidative damage, particularly when developed sustainably.[39]

The DPPH assay measured antioxidant activity by scavenging free radicals. DPPH is a stable form of free radical that appears violet and transforms to light yellow following neutralization. Green-derived CuO NPs effectively capture reactive oxygen species (ROS), as indicated by the color change in the solution. In the present study, the DPPH free radical scavenging activity was determined using a microplate reader (Skanlt RE 6.1). This study used CuO NPs at five concentrations (20, 40, 60, 80, and 100 μg mL^{-1}), as shown in Fig. 8a. It was observed that increasing the concentration of CuO NPs resulted in higher

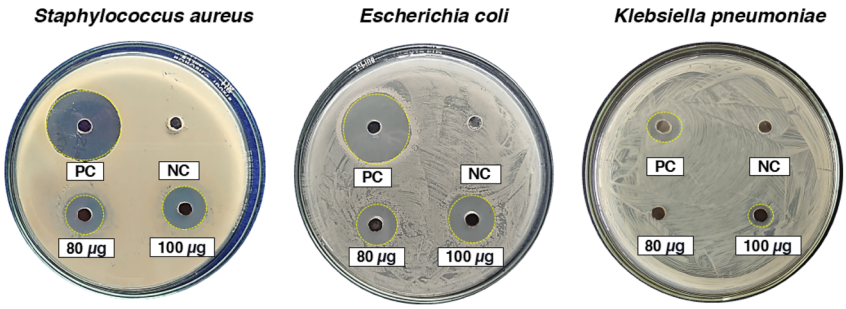

Fig. 7 Antibacterial activity of the CuO NPs at 80 and 100 μg concentrations.

Table 1 Antibacterial activity of the synthesized CuO NPs against Gram-positive and Gram-negative bacterial strains

Sample	Clinical pathogens	Zone of inhibition (mm)			
CuO NPs	*Staphylococcus aureus*	**80 μg**	**100 μg**	**PC (standard antibiotic)**	**NC (distilled water)**
	Escherichia coli	11	13	23	—
	Klebsiella pneumoniae	10	14	22	—
	Klebsiella pneumoniae	—	4	9	—

antioxidant activity in a dose-dependent manner compared with the standard antioxidant ascorbic acid. Fig. 8a shows that the DPPH scavenging effect increased from 29.19% at 20 μg mL^{-1} to 69.03% at 100 μg mL^{-1} concentration. The results indicate that CuO NPs exhibit effective antioxidative behavior. The green synthesis of CuO NPs results in the coating of antioxidants from fruit pulp extract on the NP surface. This causes DPPH to interact with CuO NPs, significantly reducing the non-radical form.

3.9. Hemolytic activity

The primary requirement for every biological material is that it must be free from negative impacts and be biocompatible. Hemolysis occurs when foreign materials come into contact with red blood cells, causing the cell membrane to rupture and release hemoglobin. When NPs are used in biological applications, they are predicted to interact with red blood cells in the bloodstream without causing any negative impact. Thus, a hemolytic assay was used to evaluate the biocompatibility of the NPs.[40] The current study employed a hemolytic assay to assess the biocompatibility of CuO NPs. The results of the hemolytic experiment revealed that CuO NPs at various concentrations (20, 40, 60, 80, and 100 μg mL^{-1}) induced only 4.38% hemolysis at 37 °C (Fig. 8b), indicating that they are biocompatible.

3.10. Electrochemical performance

3.10.1. Cyclic voltammetry analysis. The fabricated sample electrode was exposed to a cyclic voltammetry (CV) study at different scan rates from 10 to 100 mV s^{-1} in a potential window of 0.0–0.6 V in 1 M Na_2SO_4, as depicted in Fig. 9. From the plot, it is observed that there is a gradual enhancement in oxidation and reduction current with an increasing scan rate, indicating the ideal capacitive behaviour of this electrode. The shape of the CV curves at different scan rates provides insight into the charge storage mechanism of the electrode material. Furthermore, the shapes of the investigated curves are quasi-rectangular, exhibiting pseudocapacitive behaviour with some resistive limitations.[41] Furthermore, the absence of sharp redox peaks and the symmetry of the curves suggest that the electrochemical process is good in terms of reversibility and stability. This investigation proves that the material has promising characteristics for

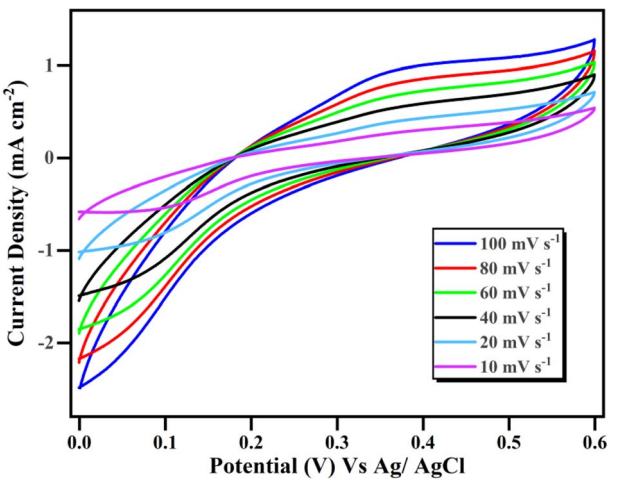

Fig. 9 Cyclic voltammetry analysis for the CuO-based electrode at different scan rates (5, 10, 20, 40, 60, 80, and 100 mV s^{-1}) in 1 M Na_2SO_4 solution.

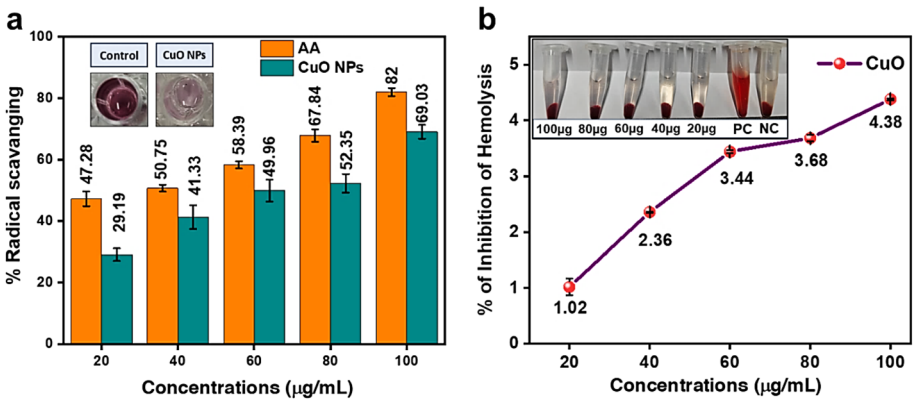

Fig. 8 (a) Antioxidant and (b) haemolytic activity of CuO NPs at concentrations of 20, 40, 60, 80, and 100 μg.

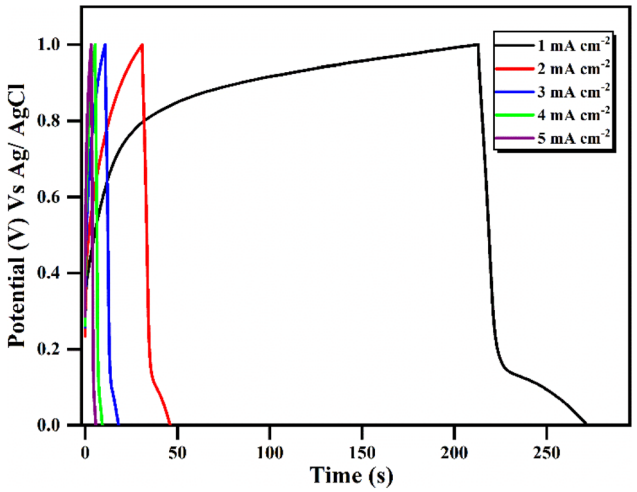

Fig. 10 GCD curves for the synthesized CuO NPs at different current densities (1.0–5.0 mA cm^{-2}).

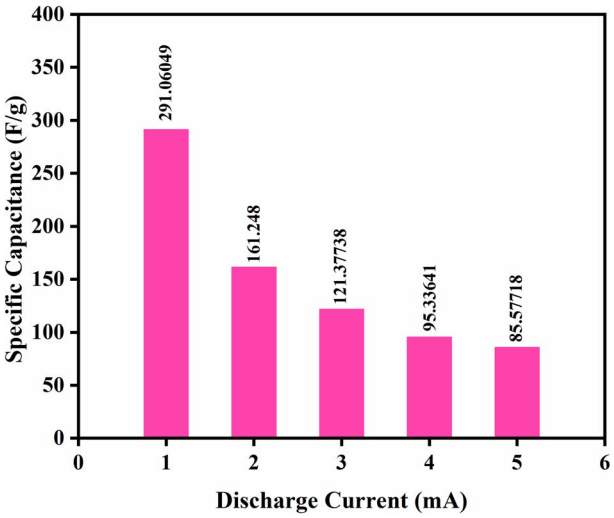

Fig. 11 Variation of specific capacitance against discharge current.

supercapacitor or energy storage applications, showing both high capacitance and fast charge–discharge ability.

3.10.2. Galvanostatic charge–discharge (GCD). Fig. 10 illustrates the GCD curves for the synthesized CuO NPs at different current densities varying from 1.0 to 5.0 mA cm^{-2}. From the graph, it is observed that with an increase in current density, a reduction in discharge time occurs due to faster charging/discharging of the electrode, giving less time to fully utilize the charge storage material. Furthermore, at higher current densities, electrode charges/discharges faster because ions have limited time to diffuse into the pores of the material. In contrast, at low current densities (1 mA cm^{-2}), the voltage profile is more linear, indicating ideal capacitive behavior. All curves are generally symmetric, indicating the excellent reversibility and electrochemical stability of the electrode. Additionally, at the beginning of the discharge, especially for higher current densities, a sharp voltage drop is observed due to internal resistance in the electrode or electrolyte. The specific capacitance of an electrode can also be investigated from the GCD using the following equation:[42]

$$C_s = \frac{I \times \Delta t}{m \times \Delta V}, \quad (4)$$

where I denotes the discharge current for the applied period Δt, m is the mass or weight of the deposited CuO, and ΔV denotes the potential window.

Variation of specific capacitance against discharge current is shown in Fig. 11. It is found that with an enhancement in discharge current, specific capacitance deteriorated because the ions have the least time to penetrate into the electrode pores, so only the outside surface contributes to charge storage. This limited ion access, along with an increased IR drop and polarization losses, reduces the specific capacitance.

3.10.3. Electrochemical impedance analysis. Electrochemical impedance spectroscopy (EIS) is a powerful tool used to understand the electrical behaviour of electrochemical systems, such as batteries, supercapacitors, fuel cells, coatings,

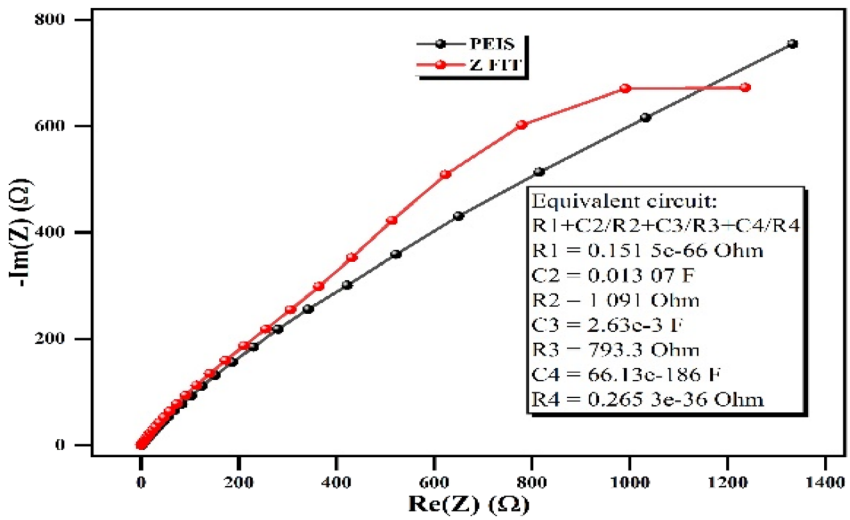

Fig. 12 Nyquist plot for the synthesized CuO NPs.

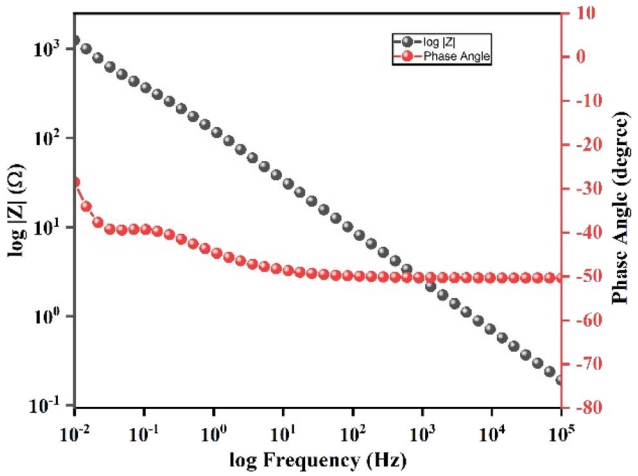

Fig. 13 Bode plot for the synthesized CuO NPs.

or corrosion processes. In this report, EIS measurements were carried out to obtain details regarding the conductive nature of the prepared CuO electrode. EIS was employed to investigate the electrochemical properties of the electrodes, which is an illustration of the real and imaginary parts of impedance spectroscopy. Fig. 12 reveals the Nyquist plot. From the plot, it is observed that, in the higher frequency region, a partial semicircle is present, indicating the occurrence of multiple overlapping electrochemical processes. Further, in the low-frequency region, the linear portion signifies the electron-transfer diffusion process within the electrode material (called Warburg impedance). Ideal electrochemical capacitors need to have the (Nyquist) plot at a line perpendicular to the real axis in a low-frequency region. However, there are deviations from the ideal behaviour ascribed to the pseudo capacitance properties of the oxide material (CuO).[43]

Fig. 13 depicts a Bode plot. From the plot, it is observed that a reduction in the magnitude of impedance with an enhancement in frequency indicates that the system offers a higher value of resistance at low frequencies and becomes more conductive at higher frequencies. Furthermore, the phase angle begins at approximately −70° and gradually shifts towards 0° as the frequency increases, confirming the transition from strong capacitive to resistive behaviour. This type of plot was important for studying electrochemical properties, including ionic conductivity, charge transfer resistance, and double-layer capacitance.

4. Conclusion

This study examines a green and eco-friendly approach for synthesizing copper oxide (CuO NPs) using *Aegle marmelos* fruit pulp extract as a natural reducing and stabilizing agent. The synthesized CuO NPs were characterized using various techniques, confirming their monoclinic phase, nanocrystalline nature, and the presence of bioactive compounds from the extract acting as capping and stabilizing agents. The antibacterial activity assays revealed significant inhibitory effects against both Gram-positive and Gram-negative bacteria. The nanoparticles also exhibited effective antioxidant behaviour and were found to be biocompatible, as determined by hemolytic assays. Furthermore, the electrochemical performance of the CuO-based electrode was investigated, showing promising characteristics for supercapacitor or energy storage applications with high capacitance and fast charge–discharge ability.

Ethical statement

The experiment involving a human blood sample was performed in accordance with the principles of the Declaration of Helsinki and was approved by the Institutional Ethics Committee of D. Y. Patil Education Society (Deemed to be University), Kolhapur. Written informed consent was obtained from the participant prior to sample collection.

Author contributions

Anil B. Patil: writing – original draft, methodology, formal analysis, data curation, conceptualization. Vaibhav B. Sankpal and Omkar S. Nille: methodology, investigation, formal analysis, data curation. Rajesh C. Waghmare: formal analysis, data curation. Vishakha S. Parkhe and Arpita Pandey-Tiwari: investigation, formal analysis, data curation. Govind B. Kolekar and Asha D. Patil: validation, supervision, review & editing. Gopinath S. Khansole: writing – review & editing, methodology, data curation, conceptualization.

Conflicts of interest

The authors declare that they have no known competing financial interests or personal relationships that could have appeared to influence the work reported in this paper.

Data availability

The datasets generated and/or analyzed during the current study are available within the article, and the raw data are available from the corresponding author upon reasonable request.

Acknowledgements

The authors gratefully acknowledge the Principal, Deshbhakt Anandrao Balwantrao Naik Arts and Science College, Chikhali, Sangli, for providing laboratory facilities, the Department of Chemistry, Shivaji University, Kolhapur (MH), India for providing characterization facilities, and the Department of Medical Biotechnology and Stem Cells and Regenerative Medicine, Centre for Interdisciplinary Research, D. Y. Patil Education Society, Kolhapur, for providing support in biomedical applications.

References

1 T. Tuutijärvi, J. Lu, M. Sillanpää and G. Chen, *J. Hazard. Mater.*, 2009, **166**, 1415–1420.
2 S. Siddiqui, R. H. Goddard and G. K. Bielmyer-Fraser, *Aquat. Toxicol.*, 2015, **160**, 205–213.
3 M. Vert, Y. Doi, K.-H. Hellwich, M. Hess, P. Hodge, P. Kubisa, M. Rinaudo and F. Schué, *Pure Appl. Chem.*, 2012, **84**, 377–410.
4 TCT Nanotech, CuO Nanoparticles of Copper Oxide, available at: **https://www.tctnanotech.com/nanotech-cuo-nanoparticles-of-copperoxide**, accessed September 2025.
5 A. Folorunso, S. Akintelu, A. K. Oyebamiji, S. Ajayi, B. Abiola, I. Abdusalam and A. Morakinyo, *J. Nanostruct. Chem.*, 2019, **9**, 111–117.
6 P. Khatereh, A. Heshmatollah and N. Mahmoud, *Ceram. Int.*, 2019, **45**, 17173–17182.
7 S. Vasantharaj, S. Sathiyavimal, P. Senthilkumar, F. L. Oscar and A. Pugazhendhi, *J. Photochem. Photobiol. B Biol.*, 2019, **192**, 74–82.
8 M. Yin, C. K. Wu, Y. B. Lou, C. Burda, J. T. Koberstein, Y. M. Zhu and S. O'Brien, *J. Am. Chem. Soc.*, 2005, **127**, 9506–9511.
9 J. Huang, S. R. Wang, Y. Q. Zhao, X. Y. Wang, S. P. Wang, S. H. Wu, S. M. Zhang and W. P. Huang, *Catal. Commun.*, 2006, **7**, 1029–1034.
10 Y. Xu, D. Chen and X. Jiao, *J. Phys. Chem. B*, 2005, **109**, 13561–13566.
11 C. T. Hsieh, J. M. Chen, H. H. Lin and H. C. Shih, *Appl. Phys. Lett.*, 2003, **83**, 3383–3385.
12 S. Venkatachalam, H. W. Zhu, C. Masarapu, K. H. Hung, Z. Liu, K. Suenaga and B. Q. Wei, *ACS Nano*, 2009, **3**, 2177–2184.
13 Q. Xu, Y. Zhao, J. Z. Xu and J. J. Zhu, *Sens. Actuators, B*, 2006, **114**, 379–386.
14 Z. E. Gahrouei, M. Imani, M. Soltani and A. Shafyei, *Adv. Nat. Sci.: Nanosci. Nanotechnol.*, 2020, **11**, 025001.
15 V. N. Sonkusare, R. G. Chaudhary, G. S. Bhusari, A. Mondal, A. K. Potbhare, R. K. Mishra, H. D. Juneja and A. A. Abdala, *ACS Omega*, 2020, **5**, 7823–7835.
16 B. Su, J. Lin, G. Owens and Z. Chen, *Environ. Pollut.*, 2020, **258**, 113668.
17 P. C. Nagajyothi, M. Pandurangan, D. H. Kim, T. V. M. Sreekanth and J. Shim, *J. Cluster Sci.*, 2017, **28**, 245–257.
18 P. Karpagavinayagam and C. Vedhi, *Vacuum*, 2019, **160**, 286–292.
19 M. V. Arularasu, J. Devakumar and T. V. Rajendran, *Polyhedron*, 2018, **156**, 279–290.
20 T. Saha, M. Bin Mobarak, M. N. Uddin, M. S. Quddus, M. R. Naim and N. S. Pinky, *Mater. Chem. Phys.*, 2023, **305**, 127979.
21 H. J. Lee, G. Lee, N. R. Jang, J. H. Yun, J. Y. Song and B. S. Kim, *Nanotechnology*, 2011, **1**, 371–374.
22 M. Valodkar, R. N. Jadeja, M. C. Thounaojam, R. V. Devkar and S. Thakore, *Mater. Chem. Phys.*, 2011, **128**, 83–89.
23 V. S. Parkhe, T. P. Patil and A. P. Tiwari, *Nanotechnol. Environ. Eng.*, 2023, **8**, 1067–1081.
24 N. Shahabadi, S. Zendehcheshm and F. Khademi, *ChemistrySelect*, 2022, **7**, e202202916.
25 J. Balcucho, D. M. Narváez and J. L. Castro-Mayorga, *Nanomaterials*, 2020, **10**, 1692.
26 S. Sivakumar, V. Sadaiyandi, S. Swaminathan and R. Ramalingam, *Biocatal. Agric. Biotechnol.*, 2024, **55**, 102983.
27 S. Jabeen, V. U. Siddiqui, S. Rastogi, S. Srivastava, S. Bala, N. Ahmad and T. Khan, *Mater. Today Chem.*, 2023, **33**, 101712.
28 S. Prakash, N. Elavarasan, A. Venkatesan, K. Subashini, M. Sowndharya and V. Sujatha, *Adv. Powder Technol.*, 2018, **29**, 3315–3326.
29 W. Mohsen, M. A. Sadek and H. A. Elazab, *Int. J. Appl. Eng. Res.*, 2017, **12**, 14927–14930.
30 H. A. Elazab, A. R. Siamaki, S. Moussa, B. F. Gupton and M. S. El-Shall, *Appl. Catal., A*, 2015, **491**, 58–69.
31 S. Jabeen, V. U. Siddiqui, S. Bala, N. Mishra, A. Mishra, R. Lawrence, P. Bansal, A. R. Khan and T. Khan, *ACS Omega*, 2024, **9**, 30190–30204.
32 D. M. Nzilu, E. S. Madivoli, D. S. Makhanu, S. I. Wanakai, G. K. Kiprono and P. G. Kareru, *Sci. Rep.*, 2023, **13**, 14030.
33 S. C. Mali, S. Raj and R. Trivedi, *Biochem. Biophys. Rep.*, 2019, **20**, 100699.
34 P. Narasaiah, B. K. Mandal and N. C. Sarada, *IOP Conf. Ser. Mater. Sci. Eng.*, 2017, **263**, 022012.
35 K. Vishveshvar, M. V. A. Krishnan, K. Haribabu and S. Vishnuprasad, *BioNanoScience*, 2018, **8**, 554–558.
36 S. V. Gudkov, D. E. Burmistrov, P. A. Fomina, S. Z. Validov and V. A. Kozlov, *Int. J. Mol. Sci.*, 2024, **25**, 11563.
37 A. N. Pham, G. Xing, C. J. Miller and T. D. Waite, *J. Catal.*, 2013, **301**, 54–64.
38 A. Sharma, H. O. Yadav and P. Bandyopadhyay, *Biophys. Chem.*, 2025, **316**, 107347.
39 A. Muthuvel, M. Jothibas and C. Manoharan, *Nanotechnol. Environ. Eng.*, 2020, **5**, 14.
40 B. Uma, K. S. Anantharaju, L. Renuka, S. Malini, S. S. More, Y. S. Vidya and S. Meena, *Ceram. Int.*, 2021, **47**, 10355–10369.
41 K. Niraj, V. Gajraj, R. Rameshbabu, R. V. Mangalaraja, N. C. Joshi and N. Priyadarshi, *Mater. Charact.*, 2022, **189**, 111991.
42 S. G. Sayyed, M. A. Mahadik, A. V. Shaikh, J. S. Jang and H. M. Pathan, *ES Energy Environ.*, 2019, **3**, 25–44.
43 A. Bello, D. Dodoo-Arhin, K. Makgopa, M. Fabiane and N. Manyala, *Am. J. Mater. Sci.*, 2014, **4**, 64–73.